

Simulation of a dust lifting process with rough walls

C.G. Ilea^{*}, P. Kosinski, A.C. Hoffmann,

*Department of Physics and Technology, The University of Bergen, Allégaten 55,
5007 Bergen, Norway*

Abstract

The aim of this paper is to present results of Eulerian-Lagrangian simulations of the dust lifting behind a shock wave in a two-dimensional domain with rough walls. Since interparticle and particle-wall collisions are important for the development of the process, simulating walls with a certain roughness is of interest influencing the trajectories of the near-wall particles, which then exchange momentum with particles higher up on the layer. Results of the simulations are shown as snapshots of particle positions at certain points in time. Comparisons between simulations with smooth walls and rough walls with varying initial dust layer thicknesses and number of particles are presented. Statistical data from the simulations are compared, such as average particle height and the number of particle-particle collisions, as is the mechanical energy lost in collisions. For the rough wall simulations, statistics relating the inclination of the virtual-wall with the emergent vertical velocity of particles and the energy lost in collisions are shown for different Gaussian distributions of angles. It was found that the general lifting effect is more intense in the rough wall simulations, the difference increasing with layer thickness. The statistical and energy data also showed significant differences between the smooth and rough wall simulations. The trends seen are substantiated by presenting some results of

simulations with a more powerful shock wave.

Key words: Dust, Explosions, Fluid mechanics, Mathematical modelling,
Multiphase flow, Simulation

1 Introduction

2 The importance of dust lifting behind shock waves and, more generally, the
3 dynamics of dense particle clouds and strands comes from applications in
4 chemical and physical engineering, in process technology and safety. Within
5 the field of process safety, organic or inorganic dust layers can be entrained
6 when an intentional or accidental pressure wave is produced in, for instance,
7 coal mines or chemical processing units. Consequently, the created dust cloud
8 combined with other substances, which may be present in the environment,
9 can form a dangerous mixture that can be easily ignited. Thus, the process
10 of dust entrainment has been the subject of numerous research efforts during
11 recent years. But, in spite of intense research, the mechanisms and phenomena
12 behind it have not been described entirely.

13 Initially, the phenomenon was studied experimentally (Fletcher, 1976; Kauff-
14 man et al., 1992; Lebecki et al., 1995). In such experiments a dust layer placed
15 on the floor of a channel is subjected to a pressure wave resulting from a pri-
16 mary explosion. The dust is entrained, dispersed in the channel and finally
17 ignited. This kind of experiments are costly, difficult to reproduce and need
18 special, very accurate measurement apparatus in order to obtain useful data.

* Corresponding author.

Email address: catalin.ilea@ifft.uib.no (C.G. Ilea).

19 The experiments, however, are not able to show in detail the phenomena in-
20 volved in the process, but only to measure some of their effects. One of the
21 main problems of experimental studies is the inability of tracking particle tra-
22 jectories accurately. In spite of these limitations, some qualitative comparisons
23 with previous experimental and numerical studies can be presented.

24 In one of the first studies (Fletcher, 1976) the shape of the lifted cloud was
25 presented and the delay time between the shock wave and this cloud was
26 estimated. In a study by Suzuki et al. (1997), experimental results showed
27 that the pressure in the dust deposit increases significantly after interactions
28 with the shock wave. Another study by Borisov et al. (1999) paid attention to
29 the visualisation of the mixture behind the shock wave. It concluded that the
30 entrained dust was not entirely dispersed in single particles due to cohesion.
31 Therefore this effect should not be neglected, especially when dealing with fine
32 particles. Fedorov and Gosteev (2002) and Fedorov and Fedorchenko (2005)
33 studied the entrainment of organic dusts behind shockwaves by modelling and
34 experimental verification. Recently, the delay in the lifting from a dust layer
35 behind a propagating shock wave and the vertical velocity of the dust cloud
36 were calculated using dust concentration measurements by Klemens et al.
37 (2006). These results are presented as useful for the validation of dust-lifting
38 models.

39 All this notwithstanding, the need for easier tools to study the process is
40 pressing and is the main driving force behind the use of numerical simulations.
41 Most of the research papers discussing such simulations, also address the issue
42 of the mechanisms responsible for the entrainment of dust and creation of a
43 particle cloud behind shock waves (Kosinski and Hoffmann, 2005; Kosinski
44 et al., 2005; Thevand and Daniel, 2002).

45 Two modelling techniques are generally used for simulating fluid-particle flows.
46 The first technique is Eulerian-Eulerian, where both phases are treated as
47 interpenetrating and interacting continua and the coupled Euler equations are
48 solved for each phase and they give the time dependent behaviour of the two
49 phases. This approach is economical, suitable for large domains and convenient
50 for implementing two-way coupling via good phenomenological models. It is
51 also the most suitable tool for engineering applications and not surprisingly
52 it is employed in numerous papers (e.g. Kosinski et al. (2005); Saito et al.
53 (2003); Samuelsberg and Hjertager (1996); Taniere et al. (2004); Thevand and
54 Daniel (2002)).

55 The second technique, increasingly used recently (e.g. Chang and Kailasanath
56 (2003); Kosinski and Hoffmann (2005); Lu et al. (2005)), is the Eulerian-
57 Lagrangian method. This approach is different in the sense that the particu-
58 late phase is not considered as a whole, but the particles are each tracked in
59 the computational domain and their motion is simulated through Newton's
60 second law of motion. Therefore, the real physical process can be simulated
61 more closely and the particle-particle and particle-wall interactions can be im-
62 plemented more conveniently. This type of model is very useful when studying
63 the fundamental physical processes behind dust lifting, e.g. in addition to in-
64 terphase drag, the effect of lift forces and particle collisions.

65 So far it has been established that inter-particle collisions are of importance
66 to the development of the process (Goldschmidt et al., 2001; Kosinski et al.,
67 2005), although this aspect has been neglected in many numerical simula-
68 tions. Also, a few studies discuss the importance and influence of lift forces
69 that appear due to inter-phase interactions (e.g. Thevand and Daniel (2002)).
70 These attempted to integrate lift forces, like the Magnus force and the Saffman

71 force, in dust-lifting models. However, these forces do not have a strict the-
72 oretical quantification and the equations used in those studies are empirical
73 with ranges of validity restricted to specific cases.

74 Turbulence is also an important factor, which affects the behaviour of particles.
75 The particles in turn influence the fluid turbulence (see e.g. Boivin et al.
76 (2000); Pascal and Oesterle (2000)). Combustion of the lifted dust is another
77 challenging issue because of the lack of basic knowledge about the complex
78 kinetic reactions (e.g. Fedorov and Gosteev (2002); Klemens et al. (2001)).

79 The aim of this paper is to simulate a dust lifting process in a 2D domain with
80 emphasis on the importance of considering wall roughness. For this, series of
81 simulations were performed with rough walls and smooth walls. Several statis-
82 tical parameters, such as the cumulative total number of collisions, the mean
83 square displacement and average height of the particles have been compared
84 between the two cases. Comparisons regarding the averaged mechanical en-
85 ergy of particles along the axes and lost energy during collisions, as functions
86 of time, have been performed.

87 As already stated, the collisions that take place between the solid particles
88 and their surroundings (walls or other particles) represent an important factor
89 influencing the process of dust lifting and entrainment. The collision algorithm
90 is particularly challenging (Sundaram and Collins, 1995) since the number
91 of solid-solid interactions is high, especially if a shock wave is present. The
92 surface roughness of the wall is also likely to be a very influential factor (Crowe
93 et al., 1998; Huber and Sommerfeld, 1998; Sommerfeld, 1992; Taniere et al.,
94 2004) because it changes the trajectories of particles interacting with the wall
95 and causes them to interact more intensely with particles higher up in the

96 layer. Two-way coupling should also be considered, since in this particle-dense
 97 system not only the gas influences the solid phase but also the particles have
 98 an significant influence on the gas flow pattern (Crowe et al., 1998).

99 **2 The mathematical model**

100 The Eulerian-Lagrangian technique for modelling two-phase flows involves
 101 solving the fluid equations in a Eulerian frame of reference (here, when the
 102 flow is a shock wave it suffices to solve the modified Euler equations rather
 103 than the full equations of motion) and the equations of motion for the particles
 104 in a Lagrangian frame of reference.

105 *2.1 Equations for the gas phase*

106 The Euler equations, modified to take into account interphase interactions,
 107 may be written as:

$$\frac{\partial \rho}{\partial t} + \nabla \cdot (\rho \vec{u}) = 0 \quad \text{conservation of mass;} \quad (1)$$

$$\frac{\partial \rho \vec{u}}{\partial t} + \nabla \cdot (\rho \vec{u}) \vec{u} + \nabla p = -\vec{f}_p \quad \text{conservation of momentum;} \quad (2)$$

$$\frac{\partial E}{\partial t} + \nabla \cdot (\vec{u}(E + p)) = -\vec{f}_p \cdot \vec{v} \quad \text{conservation of energy.} \quad (3)$$

108 The time and space dependent variables in these equations are: the gas pres-
 109 sure p , the gas density ρ , the gas velocity \vec{u} and the total energy of the gas

110 per unit volume E . The force \vec{f}_p expresses the action of the particles on the
111 unit volume of gas and \vec{v} is the velocity of the particles.

112 The volume taken up by particles is not accounted for in the gas phase equa-
113 tions. This is an approximation, since the volume fraction occupied by particles
114 is of the order of 0.1 in the initial layers (see below) and may, during the simu-
115 lation, take on even higher values locally, although it will be much lower than
116 this in most of the domain.

117 In order to close the system of equations, it is necessary to add one more
118 equation, the gas equation of state:

$$p = \rho \cdot R_g \cdot T \quad (4)$$

119 where R_g represents the specific gas constant and T is the gas temperature.
120 The gas temperature is related to its energy through the following equation:

$$E = \frac{\rho \cdot R_g \cdot T}{\gamma - 1} + \frac{\rho u^2}{2} \quad (5)$$

121 where γ is the adiabatic index of the gas.

122 *2.2 Equations for the solid phase*

123 The motion of the particles is modelled individually for each particle applying
124 Newtons second law of motion,

$$m_i \frac{d\vec{v}_i}{dt} = \vec{f}_{drag,i} . \quad (6)$$

125 Here, the variables for particle i are: m_i its mass; \vec{v}_i its velocity. The particles
 126 are moving under the influence of the drag force, $\vec{f}_{drag,i}$, which acts upon them
 127 due to the gas movement relative to them. This is calculated as:

$$\vec{f}_{drag,i} = C_D A_p \rho \frac{|\vec{u} - \vec{v}_i|(\vec{u} - \vec{v}_i)}{2} \quad (7)$$

128 where C_D represents the drag force coefficient and A_p is the projected area of
 129 the particle. The drag force coefficient C_D is a function of the relative Reynolds
 130 number, defined as:

$$Re_r = \frac{\rho d_i |\vec{u} - \vec{v}_i|}{\mu} \quad (8)$$

131 where d_i is the particle diameter, μ is the gas viscosity. The empirical for-
 132 mula of Clift and Gauvin was used to compute the drag coefficient (Clift and
 133 Gauvin, 1970).

$$\frac{C_D Re_r}{24} = 1 + 0.15 Re_r^{0.687} + 0.0175 Re_r (1 + 4.25 \cdot 10^4 Re_r^{-1.16})^{-1} \quad (9)$$

134 Due to potentially high velocity differences between gas and particles, the drag
 135 coefficient may be corrected for compressibility effects such that the particle
 136 drag coefficient not only varies with the relative Reynolds number Re_r , but
 137 also with the relative Mach number M_r . Henderson (1976) proposed such a
 138 correction, which distinguishes between three different ranges for the relative
 139 Mach number, each with its own expression for the correction. The results of
 140 this correction fits experimental data better than other available correction
 141 equations. However, in the context of the present model, its use causes prob-

142 lems with computational efficiency, due to the differences in functional form
 143 for the three Mach number ranges and the complexity of these forms. In the
 144 present model, preference was therefore given to a different correction equa-
 145 tion, namely the one proposed by Crowe et al. (1998), which also renders good
 146 results compared with other equations (Henderson, 1976). According to Crowe
 147 et al. (1998), it is necessary to correct the value of C_D for compressibility ef-
 148 fects if $M_r > 0.6$. Their proposed empirical correction is:

$$C_{D,c} = 2 + (C_D - 2)e^{-3.07\sqrt{\gamma}GM_r/Re_r} + \frac{H}{\sqrt{\gamma}M_r}e^{-\frac{Re_r}{2M_r}}$$

with :

$$G(Re_r) = \frac{1 + Re_r(12.278 + 0.458Re_r)}{1 + 11.278Re_r} \tag{10}$$

$$H(M_r) = \frac{5.6}{1 + M_r} + 1.7\sqrt{\frac{T_d}{T_c}},$$

149 where T_d and T_c are the temperatures of the particles and of the gas, respec-
 150 tively.

151 A separate issue is the modification of the drag law due to the presence of other
 152 particles in the vicinity. Gidaspow (1994) has proposed a drag law derived from
 153 Ergun's equation. This gives reasonably good results for very dense flows, best
 154 for gas volume fractions lower than 0.8. Applying such a modification to the
 155 drag law, however, requires knowledge of the local void fraction around the
 156 particle in question. Determining this void fraction in a Eulerian-Lagrangian
 157 simulation represents problems both with defining a suitable averaging volume
 158 around the particle and with computational efficiency. This is a subject which
 159 urgently requires further investigation.

160 The drag force is the only force considered in this model due to its domi-
161 nant importance compared to other forces which have a smaller effect at high
162 Reynolds numbers (Crowe et al., 1998). Also, the influence of the gas on the
163 angular velocity of the particles is not included in the particle motion model.
164 However, this parameter was calculated in the collision algorithm and changed
165 only as a consequence of particle collision.

166 *2.3 Collisions*

167 The hard-sphere model of Crowe et al. (1998) was used to model particle-
168 wall and particle-particle collisions. We give an account of the treatment of
169 particle-wall collisions here, the treatment of particle-particle collisions follows
170 the same principle.

171 The collision of a particle with a wall consists of two parts: a “compression”
172 period, where the particle compresses against the wall, followed by a “recov-
173 ery” period. A particle impacting obliquely on a wall slides along the wall
174 for the first period of the collision, and possibly stops sliding and only rolls
175 for the rest of the collision. Sliding may stop during the compression period,
176 or extend into the recovery period and then stop, or persist throughout the
177 collision.

178 Crowe et al. (1998) give alternative solutions for the emerging rotational
179 and translational velocities after the collision depending on whether the ratio
180 $v_z^{(0)}/|v|$ is larger or smaller than $-2/(7f(e+1))$, where e is the coefficient of
181 restitution for the collision (the ratio of total impulsive force, $\int F dt$, acting on
182 the particle during the compression part of the collision to that acting during

183 the recovery part), and f is the Coulombic dynamic coefficient of friction (the
 184 ratio of the normal force acting on the point of contact to the tangential one
 185 during the sliding period of the collision).

186 With our choices of e and f , which are 0.8 and 0.15, respectively, $v_z^{(0)}/|v| >$
 187 $-2/(7f(e+1))$ in all cases, and the components of the emerging velocity, \vec{v} ,
 188 and rotation $\vec{\omega}$, converted to our 2-D simulations using a coordinate system
 189 with the z -axis normal to the wall, the x -axis along the wall and the y -axis
 190 pointing out of the paper, are:

$$\begin{aligned} v_x &= v_x^{(0)} + f(e+1)v_z^{(0)} \\ v_z &= -ev_z^{(0)} \\ v_y &= v_y^{(0)} = 0 \end{aligned} \tag{11}$$

191 for the translational velocity, and

$$\begin{aligned} \omega_x &= \omega_z = \omega_x^{(0)} = \omega_z^{(0)} = 0 \\ \omega_y &= \omega_y^{(0)} - \frac{5}{d}f(e+1)v_z^{(0)} \end{aligned} \tag{12}$$

192 for the rotation vector. In these equations, the superscript (0) denotes the
 193 pre-collisional values.

194 In this paper we also look at the dissipation of mechanical energy due to
 195 collisions. This may be calculated from the above equations as follows.

196 The total translational mechanical energy of a particle is $\frac{1}{2}m\vec{v}^2$, and therefore
 197 the loss of translational energy due to a collision with a wall is:

$$E_{t,lost} = \frac{1}{2}m((\vec{v}^{(0)})^2 - \vec{v}^2). \quad (13)$$

198 Inserting the components for the vectors from Equation (11) and simplifying
 199 gives:

$$E_{t,lost} = \frac{1}{2}m \left[(v_z^{(0)})^2(1 - e^2 - f^2(1 + e)^2) - 2v_x^{(0)}v_z^{(0)}f(1 + e) \right]. \quad (14)$$

200 The total rotational mechanical energy of a particle is $\frac{1}{2}I\vec{\omega}^2$, where I is the
 201 particle's moment of inertia, which for a spherical particle is $\frac{2}{5}m(\frac{d}{2})^2$, and the
 202 loss of rotational mechanical energy during a wall collision is, therefore:

$$E_{r,lost} = \frac{1}{2}I((\vec{\omega}^{(0)})^2 - \vec{\omega}^2). \quad (15)$$

203 Inserting from Equation (12) and simplifying gives:

$$E_{r,lost} = \frac{1}{2}I \left[-\left(\frac{5}{d}f(1 + e)v_z^{(0)}\right)^2 + 2\omega_y^{(0)}\frac{5}{d}f(e + 1)v_z^{(0)} \right]. \quad (16)$$

204 The total loss of mechanical energy is $E_{t,lost} + E_{r,lost}$. While $E_{t,lost}$ can be
 205 studied in the x and z -directions separately, $E_{r,lost}$ cannot.

206 2.4 Modelling of wall roughness

207 The roughness of walls can be modelled in two general ways (Crowe et al., 1998;
 208 Sommerfeld, 1992), as special functions, that describe the topology of hard
 209 boundary of the domain, or as random inclination angles of the contact point
 210 between the particle and the wall. The latter, called the "virtual wall" model

211 (see Figure 1), was used in this research as described in references (Crowe
 212 et al., 1998; Huber and Sommerfeld, 1998; Sommerfeld, 1992; Taniere et al.,
 213 2004). In accordance with this, any time a particle-wall collision was detected,
 214 a random inclination angle α was generated and the local coordinate system
 215 was rotated by α . The hard sphere model was next applied to determine the
 216 post-collisional motion of the particle. Finally, the results were re-transformed
 217 back in the original coordinate system (Taniere et al., 2004).

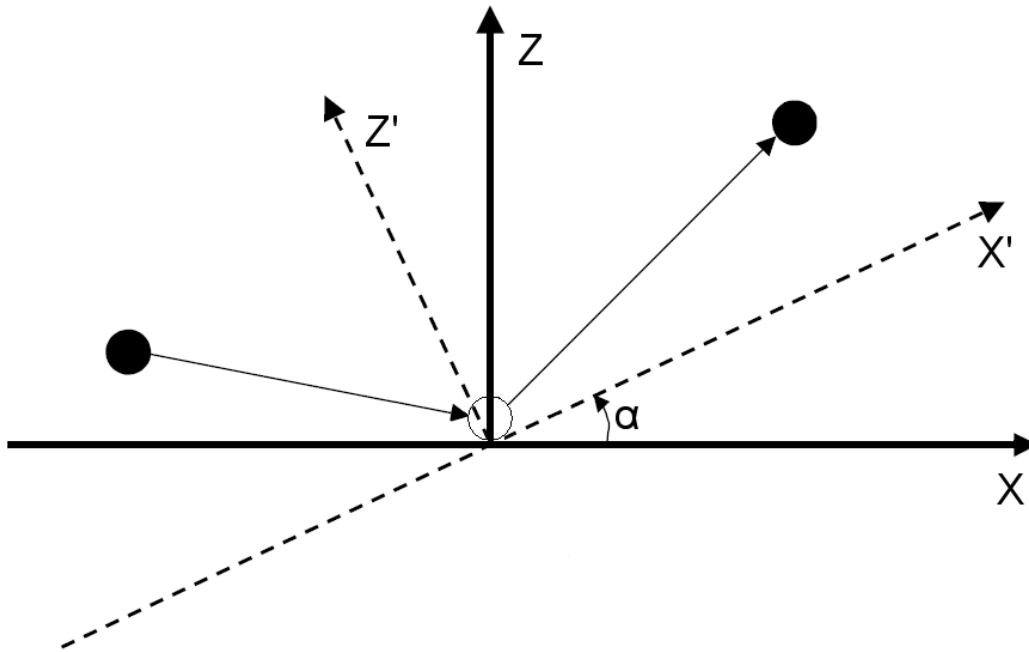


Fig. 1. The "virtual-wall" model for roughness

218 There are two possible problems that might arise in such an approach. Firstly,
 219 after rotating the coordinate system, before applying the collision model, it
 220 is possible to obtain velocity vectors that actually point away from the wall.
 221 Particles are actually moving away from the inclined "virtual wall" instead of
 222 toward it. This is the so-called "shadow effect" (Huber and Sommerfeld, 1998;
 223 Sommerfeld, 1992; Taniere et al., 2004). Secondly, a similar case can arise after
 224 the post-collisional values are calculated and the results are transformed back
 225 in the normal coordinate system. The post-collisional velocity vectors might

226 still be pointing toward the wall and not away from it. Therefore, the angle
 227 values that generate this problem should not be considered.

228 A study by Sommerfeld (1992) presents a comparison between three roughness
 229 models, which basically differ in the random angle value generator. It was in
 230 that paper concluded that a Gaussian random number generator rendered the
 231 best results compared to experimental data.

232 2.5 Numerical techniques

233 2.5.1 Solving the flow equations

234 To solve the Euler equations given a sharp shock initial condition, a proper
 235 numerical technique must be used. A second-order flux corrected transport
 236 algorithm (LCPFCT) was implemented (Boris et al., 1993). This method has
 237 been used before for similar problems (e.g. Chang and Kailasanath (2003)). In
 238 accordance with the Lagrangian approach, the particles are treated as point-
 239 like objects and their behaviour is simulated according to the forces that act
 240 upon them. The positions of each particle and their velocities are calculated
 241 every time-step. The numerical scheme for the particle flow is:

$$m_i \frac{\vec{v}_i^{n+1} - \vec{v}_i^n}{\Delta t} = C_D A_p \rho \frac{(\vec{u}^{n+1} - \vec{v}_i^{n+1}) |\vec{u}^n - \vec{v}_i^n|}{2} \quad (17)$$

$$\vec{r}_i^{n+1} = \vec{r}_i^n + \Delta t \frac{(\vec{v}_i^{n+1} + \vec{v}_i^n)}{2}. \quad (18)$$

242 The index i identifies each particle, n is the time-step index and \vec{r}_i is the
 243 position vector. [The 2-way coupling terms mentioned in equations 2 and 3,](#)

244 which link the solid phase to the gas phase, are determined by adding the
245 effects of each particle that is located inside a specific cell.

246 2.5.2 Dealing with collisions

247 An event-driven algorithm (Sundaram and Collins, 1995) were adopted in
248 order to properly account for collisions. The purpose of the event-driven algo-
249 rithm is to detect the instant of occurrence of each collision within a time-step
250 in order for all of them to be treated in a proper sequential manner. Figure 2
251 presents the steps followed by the event-driven algorithm. At the beginning
252 of each time-step the variables of the particles are advanced to the full length
253 of the time-step. At this point particles are checked for overlaps, i.e. if the
254 distance between two particles is less the the sum of 2 particle radii or the
255 distance between one particle and a wall is less than one particle radius, then
256 a collision has to be taken into account in the time passed. So, if this is the
257 case, it is necessary to calculate the instant of time when the collision actually
258 took place. In order to do this, we assume that the particles are advancing
259 with a constant speed within the time step, equal to the average between the
260 initial and final velocity value. The quadratic equation:

$$|\vec{r}_{ij} + \Delta t_{ij}^c \cdot \vec{v}_{ij}| = 2 \cdot r_p \quad (19)$$

261 was solved when dealing with inter-particle collisions. The initial relative dis-
262 tance vector between particles i and j is \vec{r}_{ij} , the relative speed of the pair is \vec{v}_{ij}
263 and r_p is the particle radius. This equation cannot be solved along one of the
264 axis, as linear, because the component length of the allowed distance between
265 the particles cannot be estimated. Thus, one gets two solutions for the time

266 of collision Δt_{ij}^c and the smaller positive value is chosen and compared with
 267 values calculated for other particle pairs in order to check for the minimum
 268 value of collision time. This is done in order to finally obtain the instant in
 269 time for the first collision.

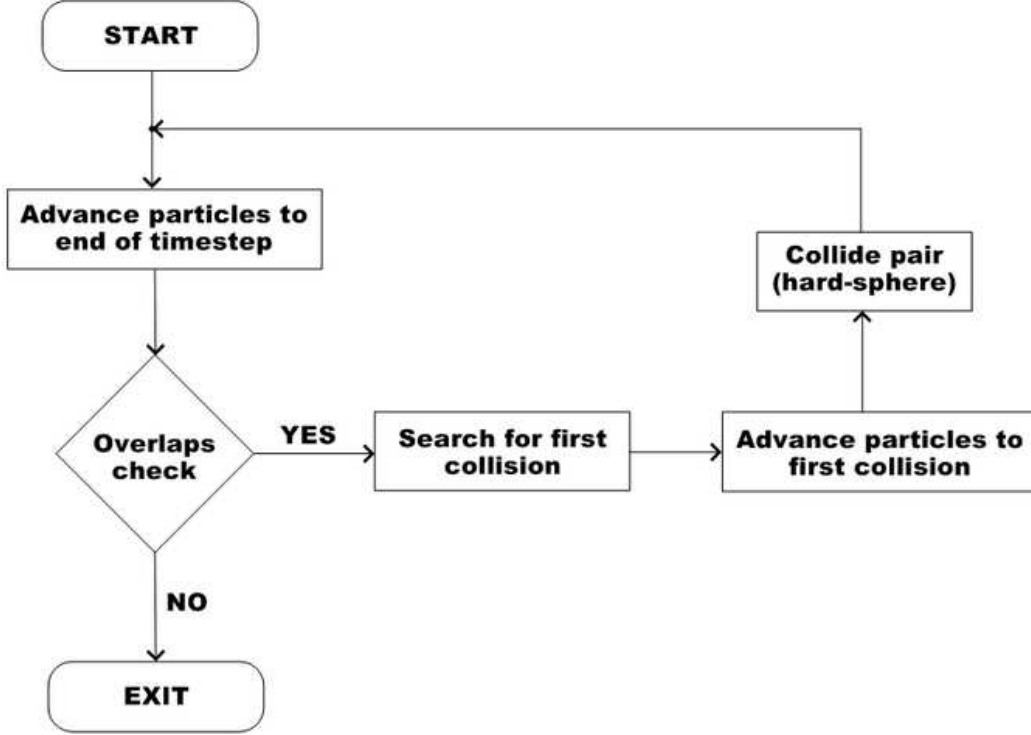


Fig. 2. The event-driven algorithm

270 The linear equation:

$$d_{i,w} + \Delta t_{iw}^c \cdot |\vec{v}_i| = 0 \quad (20)$$

271 is solved in the case of particle-wall collisions. Here, $d_{i,w}$ represents the distance
 272 that particle i has to cover from the initial position until it touches the wall,
 273 \vec{v}_i represents the average velocity of particle i taken constant for this time
 274 interval and Δt_{iw}^c is the unknown time of collision. It is important to mention
 275 that the overlap check was initially done for each possible pair of particles, thus

276 rendering a long computation time. But, using the so-called neighbour lists
277 (Sundaram and Collins, 1995) made the algorithm quicker without missing
278 any of the collisions.

279 Knowing when the first collision occurs, all the particles are advanced to their
280 position at that time. The actual collision is now taken into consideration and
281 the hard-sphere model is called to calculate the post-collisional linear and an-
282 gular velocities of the colliding particles. In the model, particle deformation is
283 neglected and the friction between solids obeys Coulombs law (Crowe et al.,
284 1998). The coefficient of restitution, defined as the ratio between the post-
285 collisional and the pre-collisional velocities normal to the plane of impact is
286 very important to the behaviour of the particles and can vary between 0 (for
287 non-elastic collision) and 1 (for fully elastic collisions). The Coulombic friction
288 coefficient for two solid bodies in contact is also significant when accounting
289 for inter-particle and particle-wall collisions. The values of the restitution co-
290 efficient and the friction coefficient are specified as constants throughout the
291 simulation.

292 Finally, the sequence is started again from the time of the first collision. The
293 loop will run until no more overlaps are found during the entire time-step and
294 the whole algorithm will start again at the next time-step.

295 3 Results & Discussion

296 3.1 Simulations with a 4 bar shock wave

297 For simulation purposes, the chosen grid was uniform along both axes and the
298 computational cell was represented by a square. The LCPFCT algorithm was
299 tested for grid sensitivity. The height of the domain was 1 cm and the length
300 of the domain was 30 cm. For all simulations the length of the computational
301 square cell was 0.25 mm. The boundary values of the fluid density, pressure
302 and velocity components were set the same as in the first/last cell of the actual
303 domain, respectively, with the exception of the fluid velocity component that
304 is normal to the boundary. Mirror boundary conditions were employed for
305 these cases. Air was chosen as the fluid phase. In order to obtain an initial
306 shock wave, the domain was split into 2 regions, a high pressure region and
307 a low pressure one, divided by a membrane at 2 cm along the x axis. When
308 removing the membrane, the shock wave will start propagating. A pressure
309 difference of 4 bar was set for all dust lifting simulations and this produced a
310 shock wave moving at a Mach number of 1.34. The velocity of the shock wave
311 was aprox. 460.2 m/s.

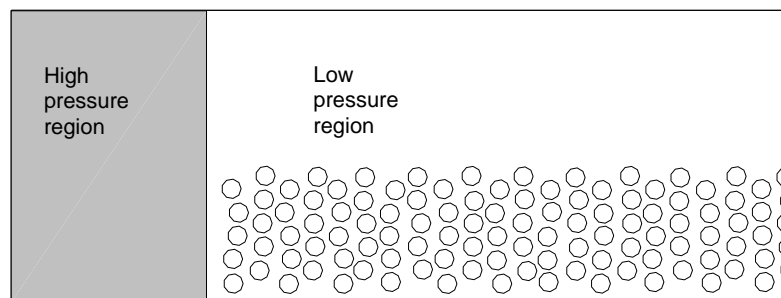


Fig. 3. Example of particle placement and simulation domain

312 The particle layer was placed right in front of the shock wave. Particles were
313 initially placed in regular arrays. Their positions were then altered by a ran-

314 dom value in both coordinate directions, in order to obtain a random initial
 315 placement of particles in a compact layer. An example of such a domain and
 316 particle placement is given in Figure 3. The length of the layer was the same
 317 for all simulations, i.e. 1.35 cm. Simulations were performed for layers with
 318 different thicknesses. Firstly, 500 particles were simulated, than 700 and fi-
 319 nally 900 particles, with layer thicknesses of 0.75 mm, 0.99 mm and 1.23 mm,
 320 respectively. All particles were considered spherical and identical with a 100
 321 μm diameter and a density of 1000 kg/m^3 . The average number of particles
 322 per computational cell was approximately 3.

323 Regarding the collision models, the values of the friction coefficient and of
 324 the restitution coefficient were set to 0.15 and 0.8, respectively, in accordance
 325 with suggestions made in Goldschmidt et al. (2001). The random angle val-
 326 ues necessary for simulating the rough walls were obtained using a Gaussian
 327 random number generator algorithm as suggested in Press et al. (1992) with
 328 a standard deviation of 10 degrees and a mean value of zero.

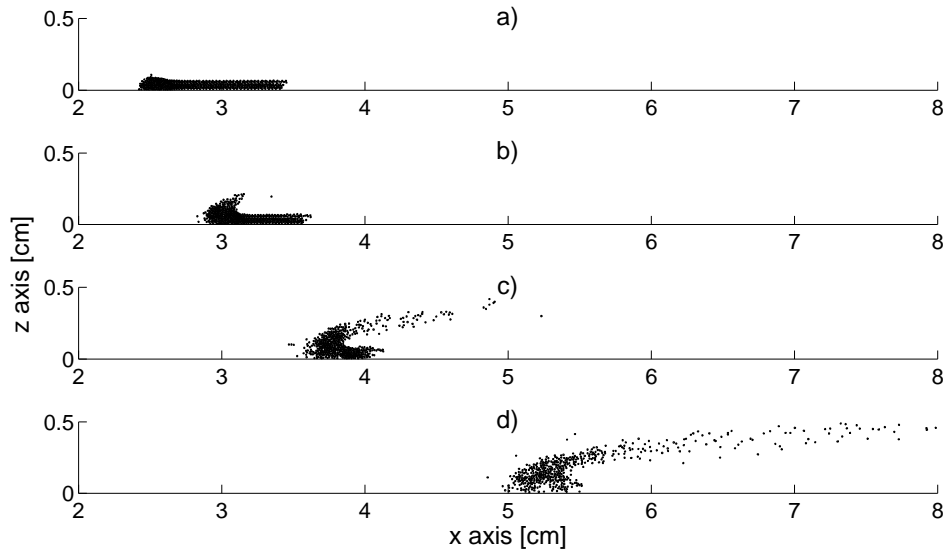


Fig. 4. Evolution of a dust lifting process of 500 particles with rough walls after approx.: a) 0.3 ms; b) 0.5 ms; c) 0.8 ms and d) 1.2 ms

329 Three different simulations were performed for the smooth wall model and
330 three for the rough wall model, for each initial layer thickness. Figure 4
331 presents the evolution in time of the dust lifting process of 500 particles for one
332 of the rough wall simulations. The entrainment of the particles in the direc-
333 tion of the wave can be observed. Early snapshots of particle positions indicate
334 that, while particles are blown off from the top of the layer by the wave, within
335 the layer they seem to shield each other from the effects of the gas flow. These
336 observations are valid for the other layer thicknesses as well, except that the
337 entrainment effect is less intense due to the larger number of particles. [The](#)
338 [dust layer snapshots presented in Figure 4 show profiles that are qualitatively](#)
339 [similar to the ones presented by Fedorov and Fedorchenko \(2005\) or Kosin-](#)
340 [ski and Hoffmann \(2005\). Some studies e.g. \(Fedorov and Fedorchenko, 2005\)](#)
341 [present results where the layer surface exhibits some "humps". These can ap-](#)
342 [pear due the reflection of the shock wave in the layer and from the bottom wall.](#)
343 [In our simulations this has not taken place mainly due to the small length of](#)
344 [the initial layer. For the same reason, the detailed shock wave structure inside](#)
345 [the layer is difficult to ascertain.](#)

346 Comparing the fronts of the layers at the end of such simulations, for a smooth
347 wall simulation (Figure 5a) and for a rough wall simulation (Figure 5b), dif-
348 ferences can be observed. In smooth wall model, particles seem to gather up
349 while remaining in the roughly layered configuration of the initial arrange-
350 ment. They interact mostly along the direction of the wave. The shock wave
351 has brought the particles closer to each other and due to the lack of a verti-
352 cal velocity component they present this arrangement. However, in the rough
353 wall model, they are more mixed and no visible alignment of particles can be
354 observed. The vertical component of particle velocity has a larger value due

355 to the collisions with the rough bottom wall. The latter model seems the more
 356 physically plausible.

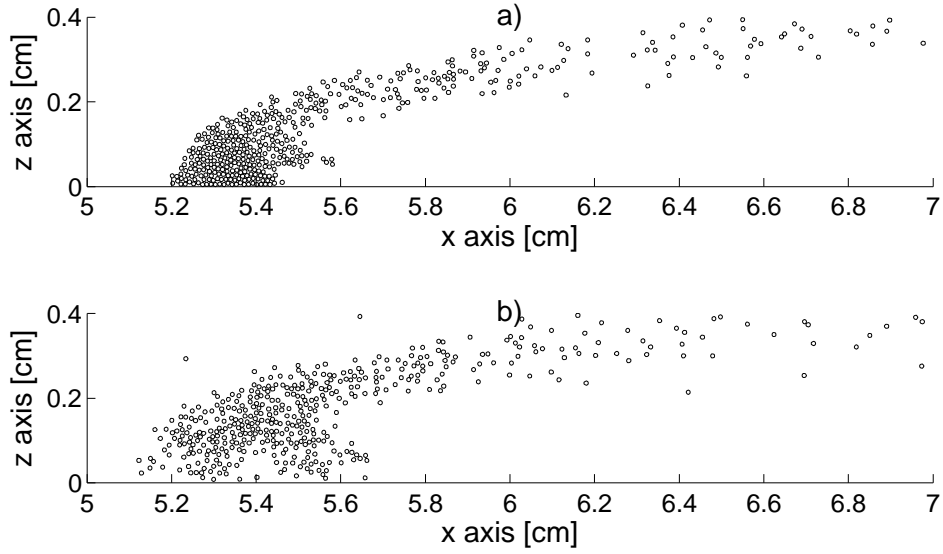


Fig. 5. Front of the 500 particle layer for the: a) smooth wall; b) rough wall simulations after approx. 1.2 ms

357 To further compare the two models, the average height of the particles was
 358 calculated as a function of time, according to:

$$h(t) = \frac{1}{N} \sum_i z_i(t) \quad (21)$$

359 where N is the total number of particles, z_i represents the particle elevation.
 360 This parameter is plotted against time in Figures 6a, 7a, 8a, where the letter S
 361 denotes the smooth wall simulations and R is for rough wall simulations. It can
 362 be noticed that, by the end of the simulation, the rough wall model indicates
 363 bigger average height values. The differences between the two models are more
 364 visible as the initial layer is thicker. The lifting effect in these simulations is
 365 mainly due to the collisions that take place in the layer.

366 Figures 6b, 7b and 8b present the time dependence of the cumulative number

367 of collisions for all the simulations. This shows a considerably larger number
 368 of collisions in the smooth wall simulations. This seems to be in contradiction
 369 with the statements above. The reason for this is that during the smooth wall
 370 simulation, the particles are brought close to each other by the on-coming air,
 371 while still being aligned in layers. Due to this, they will collide repeatedly.
 372 These collisions however will not give the particles a significant vertical com-
 373 ponent of velocity and therefore will not contribute significantly to the lifting
 374 effect. In the rough wall model, on the other hand, the particles in the layer
 375 closest to the wall receive a significant vertical velocity component and will
 376 exchange momentum with the particles higher up in the layer giving rise to a
 377 certain mixing, breaking the particle alignment.

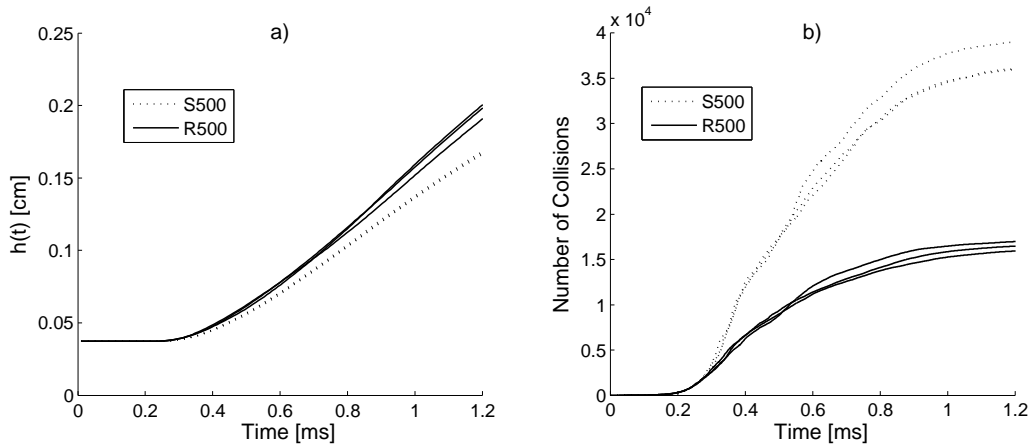


Fig. 6. a) Average height of particles; b) The cumulative number of collisions. Case of 500 particles

378 Figures 9, 10 and 11 present the average mechanical energy of the particles
 379 along the two axes x and z , respectively, as functions of time. These were
 380 calculated by summing the translational energies of all the particles, at each
 381 time step, and averaged over the total number of particles. Comparing the two
 382 models, it can be stated that the rough wall model presents a slightly larger
 383 mechanical energy value in both cases. But a more significant difference, from

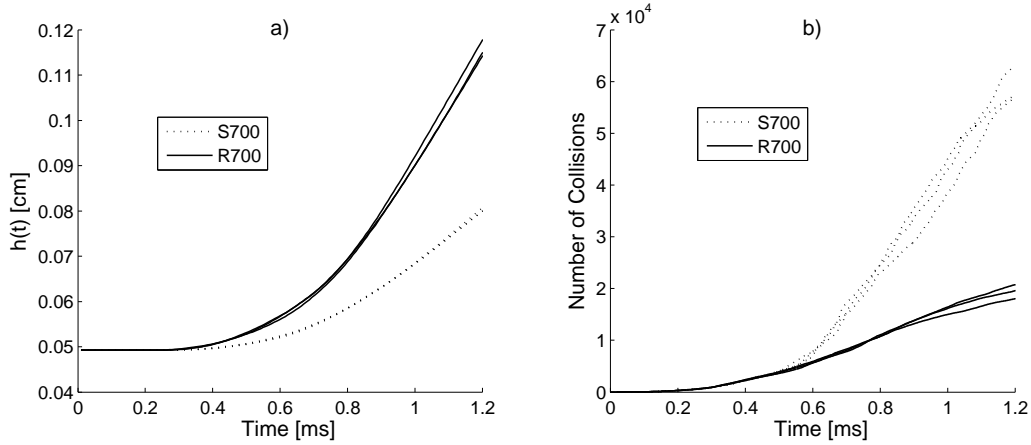


Fig. 7. a) Average height of particles; b) The cumulative number of collisions. Case of 700 particles

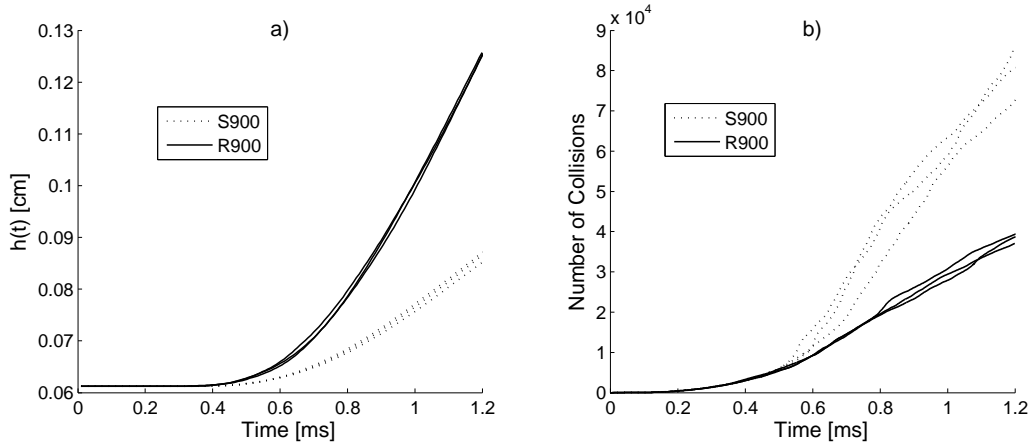


Fig. 8. a) Average height of particles; b) The cumulative number of collisions. Case of 900 particles

384 a mechanical energy point of view, can be noticed in Figure 12 where the
 385 energy lost during particle collisions is plotted as a function of time. The
 386 translational and rotational energy lost in each collision was summed at each
 387 time step and plotted versus the time scale. It can be noticed that the rough
 388 wall model presents higher lost energy values which concur with the earlier
 389 statements, that even though the total number of collisions is small compared
 390 to the smooth wall model, they are stronger and therefore more mechanical
 391 energy consuming. As a consequence particles interact more vigorously with
 392 the solid environment around them. The thickness of the initial layer does not

393 seem to add a specific effect to the mechanical energy analysis other than the
 394 fact that if more particles are present, the number of collisions is higher and,
 395 consequently, the total energy lost in collisions is bigger.

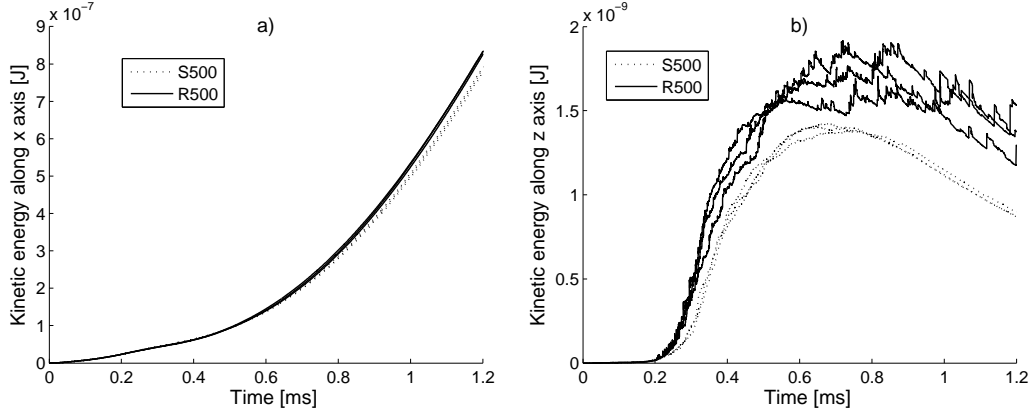


Fig. 9. Average mechanical energy per particle along the: a) x axis; b) z axis. Case of 500 particles.

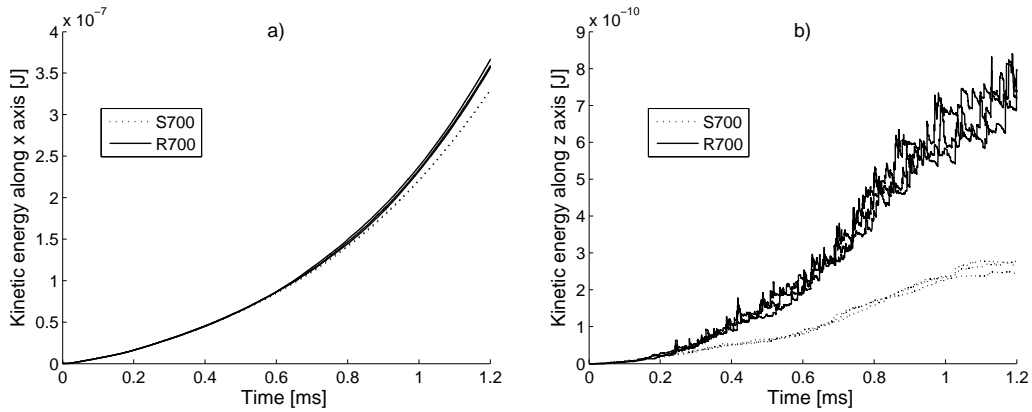


Fig. 10. Average mechanical energy per particle along the: a) x axis; b) z axis. Case of 700 particles.

396 Figures 13a, 14a, 15a and 16a present the dependence of the vertical veloc-
 397 ity of particles after collisions with rough walls on the virtual-wall inclina-
 398 tion angle. The four charts correspond to different standard deviations of the
 399 Gaussian random number generator. As expected, values of inclination give
 400 increasing vertical velocity to particles, giving rise to increased inter-particle 2-
 401 momentum exchange in the z-direction. The angle value distribution is shifted
 402 toward more positive values, with increasing standard deviation. This is due to

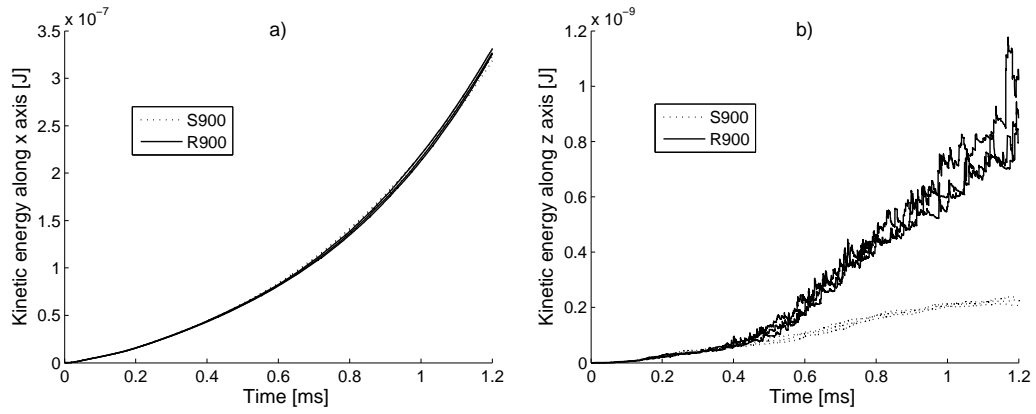


Fig. 11. Average mechanical energy per particle along the: a) x axis; b) z axis. Case of 900 particles.

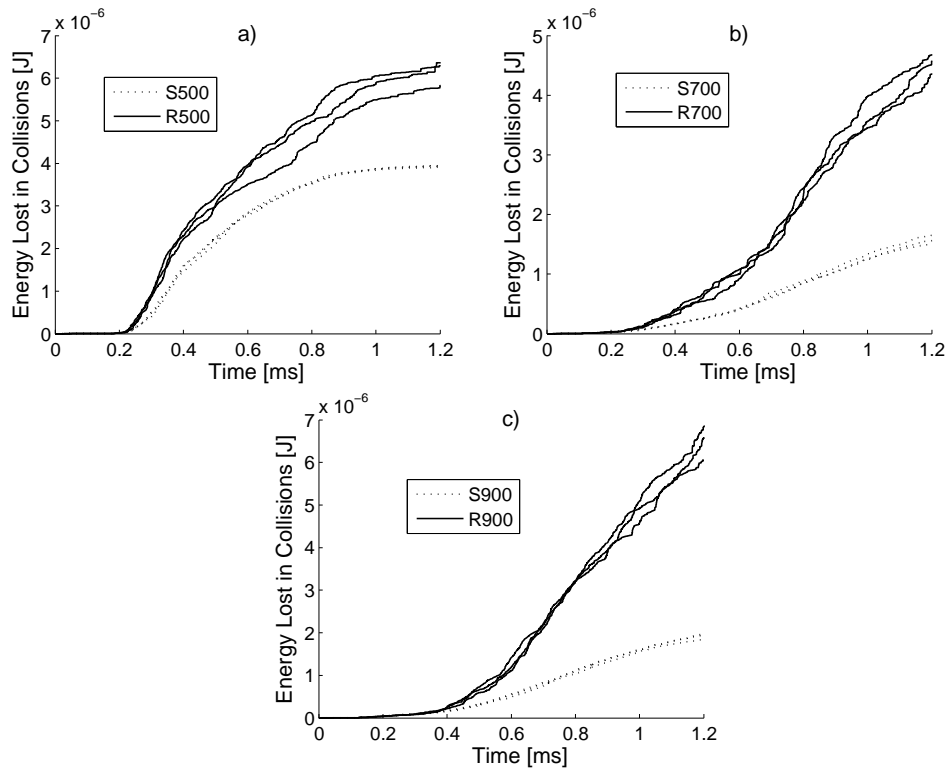


Fig. 12. Total lost mechanical energy by particles during collisions: a) 500 particles; b) 700 particles; c) 900 particles.

403 values which induce the shadow wall effect during simulations being discarded.

404 Figures 13b, 14b, 15b and 16b present the dependence of the mechanical energy

405 lost by the particles during wall collisions, on the rough wall angle, for the same

406 standard deviations of the random number generator. A similar trend can be
407 observed here. For higher, both positive and negative, inclination angles the
408 amount of energy that the particles lose in wall collisions increases.

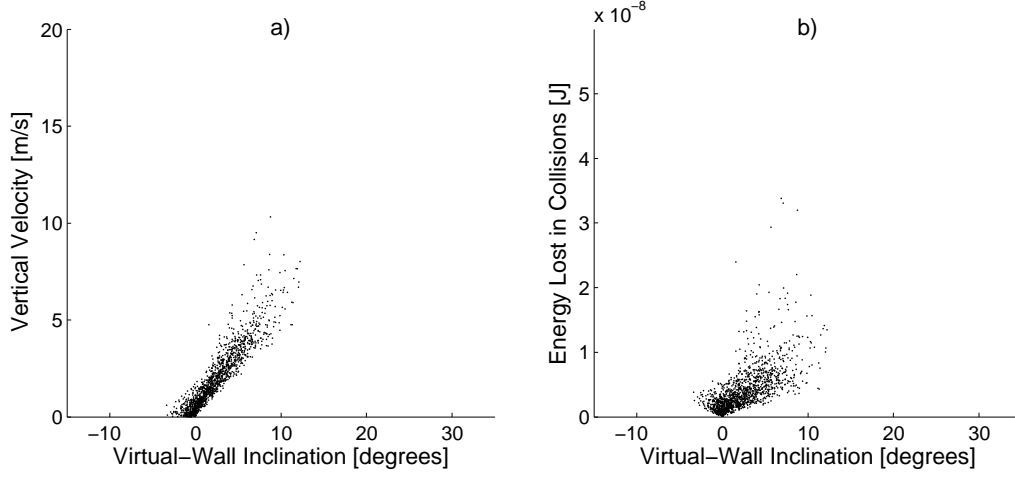


Fig. 13. a) Emergent vertical velocity of particles; b) Lost mechanical energy after collisions with rough walls. Standard deviation of wall inclination angle: 4 degrees.

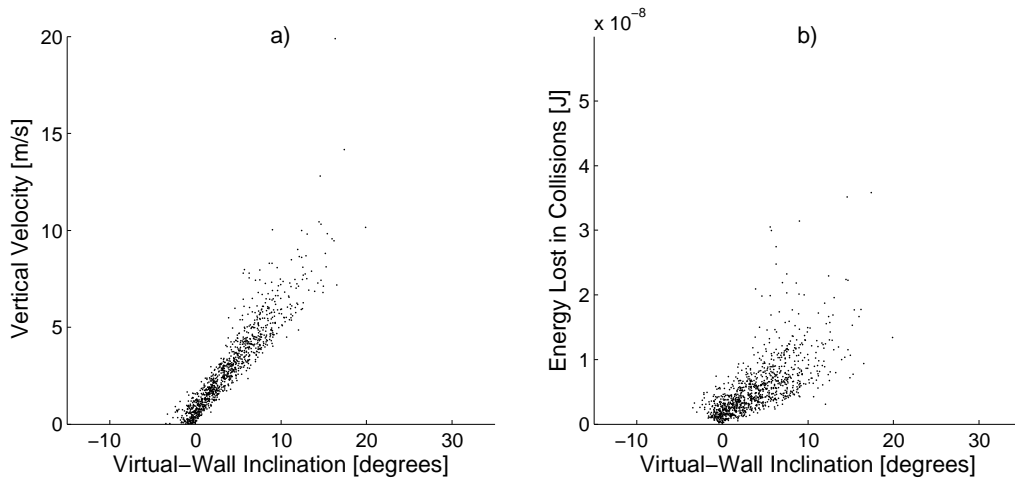


Fig. 14. a) Emergent vertical velocity of particles; b) Lost mechanical energy after collisions with rough walls. Standard deviation of wall inclination angle: 6 degrees.

409 Simulations with different initial volume fractions were also carried out using
410 the rough wall model. The same number of particles, i.e. 500, was used for
411 these simulations. The length of the layer was kept the same as before but
412 the particles were placed slightly looser or tighter in the vertical direction in
413 order to obtain two other initial values of volume fractions. The results are

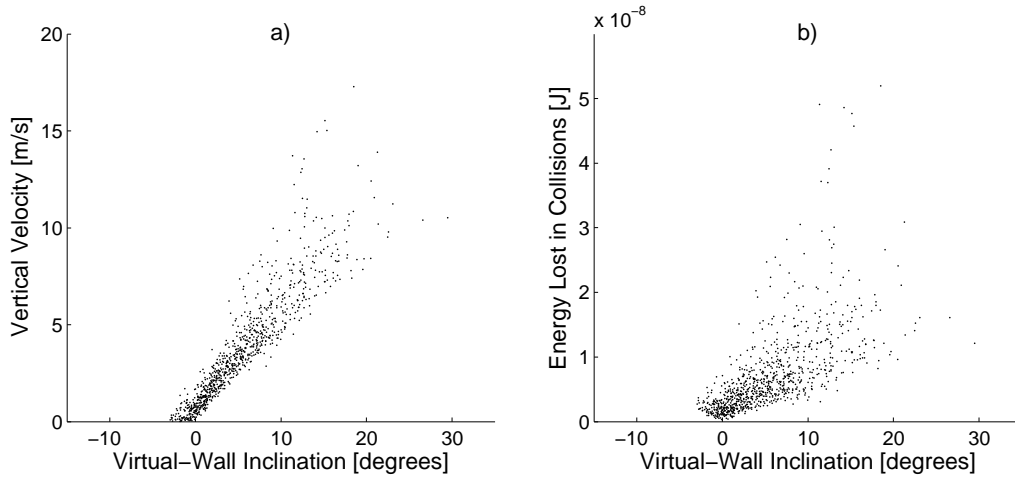


Fig. 15. a) Emergent vertical velocity of particles; b) Lost mechanical energy after collisions with rough walls. Standard deviation of wall inclination angle: 8 degrees.

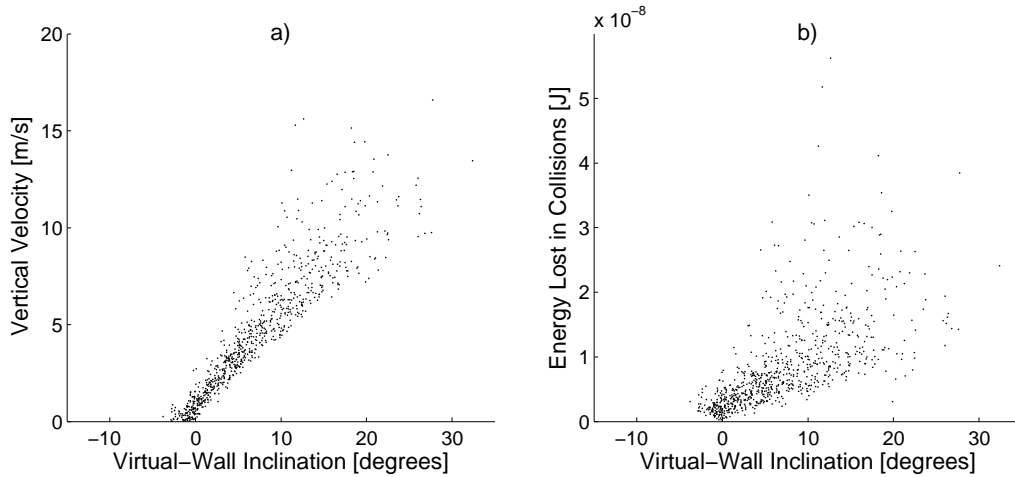


Fig. 16. a) Emergent vertical velocity of particles; b) Lost mechanical energy after collisions with rough walls. Standard deviation of wall inclination angle: 10 degrees.

414 presented in Figure 17. It can be observed that in the case where the particles
 415 are packed closer to the wall, higher values of the average height are obtained
 416 towards the end of the simulated time. Conversely, particles that initially are
 417 placed more loosely will more easily be blown by the shock wave, will collide
 418 less, and will not be lifted as much. The same trend is expected from smooth
 419 wall simulations.

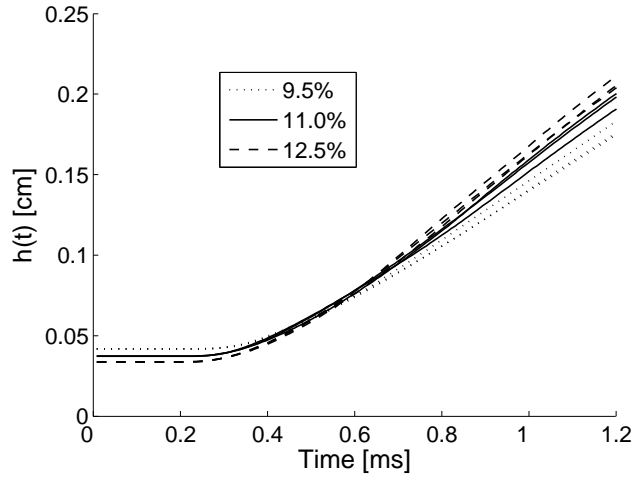


Fig. 17. Average height of particles for different volume fractions of the initial layer. Simulations of 500 particles with rough walls.

420 *3.2 Simulations with a 40 bar shock wave*

421 The remarks made previously on simulations using a less powerful shock wave
 422 were confirmed when studying results from simulations of more intense shock
 423 waves. Figures 18 - 21 present statistical results of dust lifting process simula-
 424 tions, using an initial pressure difference of 40 bar, which resulted in a shock
 425 wave moving at a Mach number 2.05, with a velocity of 707.5 m/s. The already
 426 stated effects are more pronounced in all these charts.

427 **4 Concluding remarks**

428 Concluding, a rough wall model gives significant changes in the simulation re-
 429 sults compared to smooth wall simulations. The general lifting effect appears
 430 more intense in the rough wall model as the average height values correspond-
 431 ing to this model are bigger. Even though the number of collisions is higher
 432 for the smooth wall model, the many repeated collisions between neighbouring

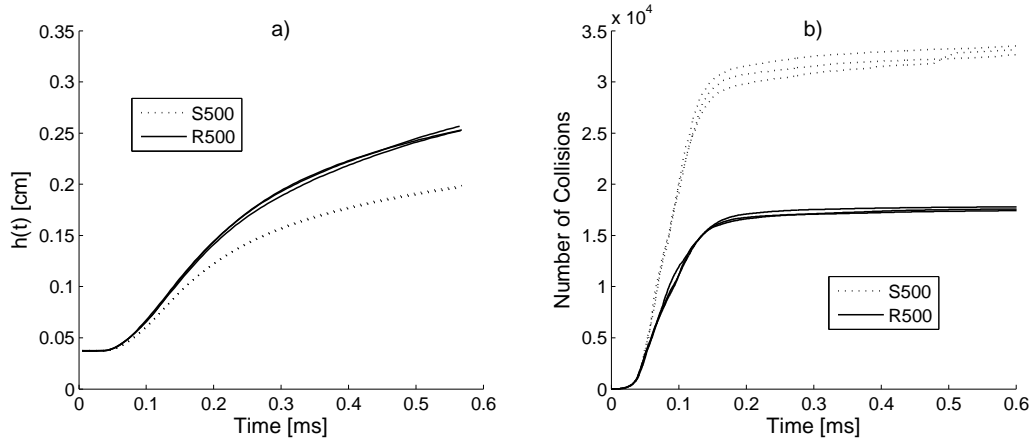


Fig. 18. a) Average height of particles; b) The cumulative number of collisions. Case of 500 particles. Shock wave Mach number 2.05.

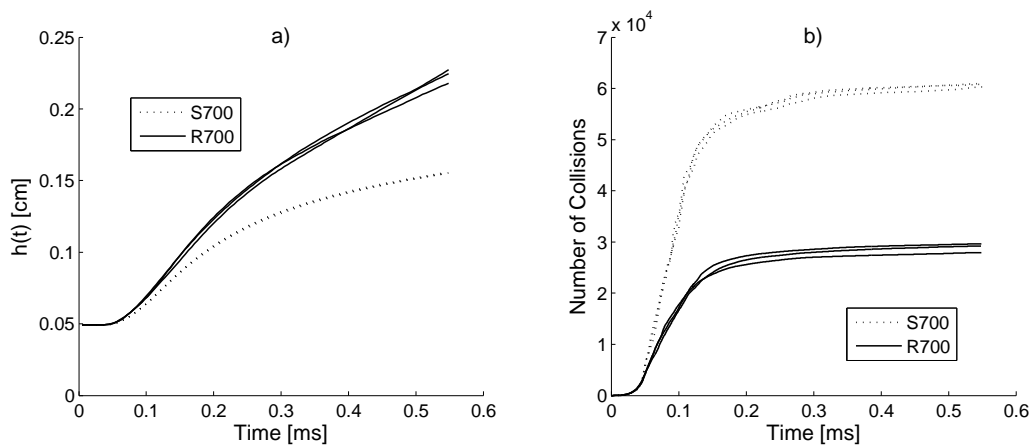


Fig. 19. a) Average height of particles; b) The cumulative number of collisions. Case of 700 particles. Shock wave Mach number 2.05.

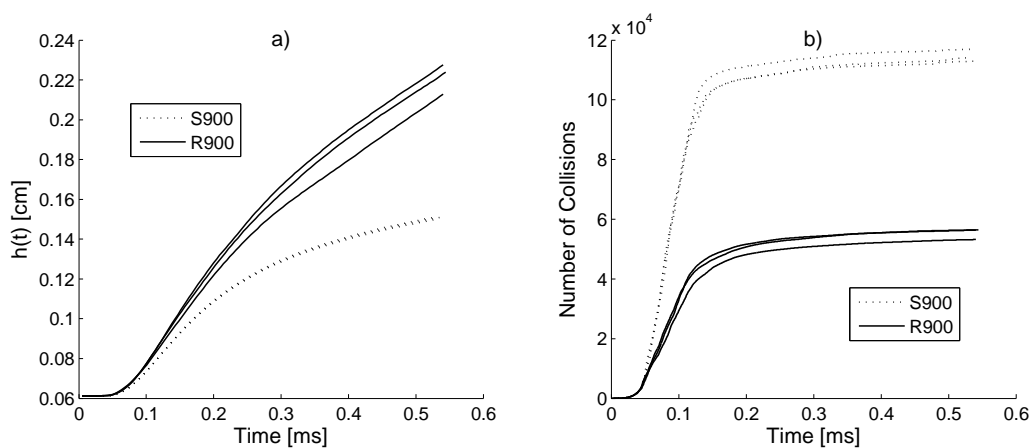


Fig. 20. a) Average height of particles; b) The cumulative number of collisions. Case of 900 particles. Shock wave Mach number 2.05.

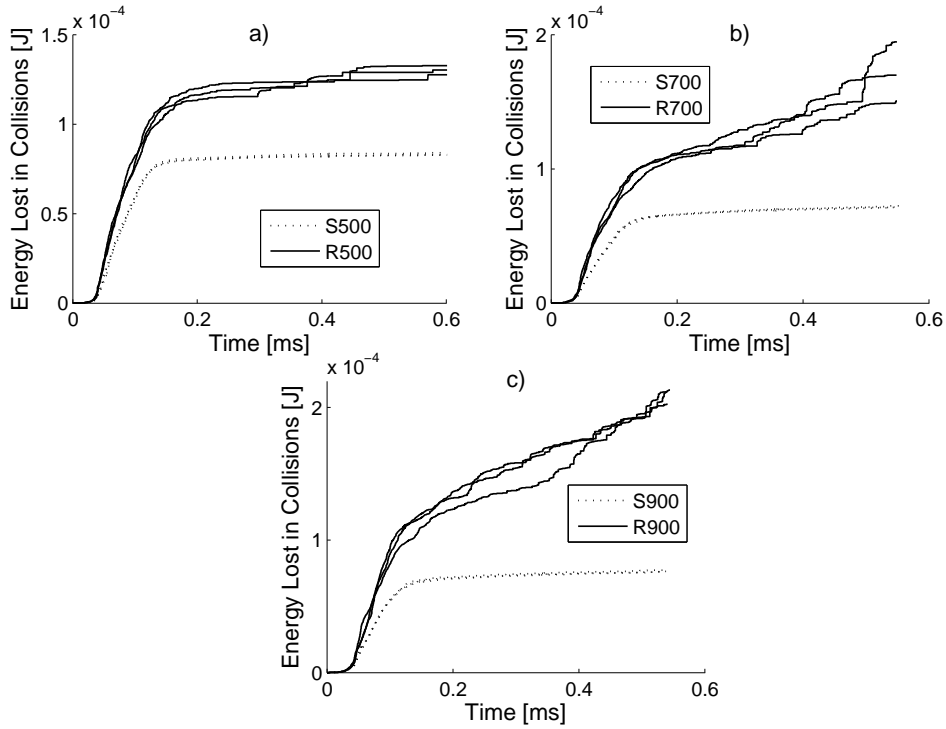


Fig. 21. Lost energy by particles during collisions. Shock wave Mach number 2.05:
a) Case of 500 particles; b) Case of 700 particles; c) Case of 900 particles.

433 particles within the same layer in the smooth wall model do not contribute to
434 the lifting effect. This is confirmed when comparing data regarding the average
435 mechanical energy of particles and lost energy of particles due to collisions.
436 These effects are more pronounced as the initial simulated shock wave is more
437 powerful.

438 Statistics regarding the dependence of the post-collisional vertical velocity
439 of particles and energy loss during rough wall collisions, on the inclination
440 of the virtual wall are also presented. These results showed that increasing
441 values of wall inclination angles have a significant influence on both parame-
442 ters. Particles are able collide stronger with the wall, more energy consuming
443 and emerge from collisions with increasing vertical velocity. This effect leads
444 to increased inter-particle 2-momentum exchange in the z-direction. Using a

445 Gaussian random number generator with higher standard deviation values will
446 render a broader angle distribution and, thus, the wall roughness effects are
447 more obvious.

448 Overall, it can be stated that a rough wall model should be employed in dust
449 lifting simulations and be subjected to experimental validation.

450 We list what we see as the most important activities to improve this approach
451 further. The model itself can be improved in a number of ways, the most
452 important of which is implementing a drag law that can describe the motion of
453 particles more accurately. Finding or performing experimental measurements
454 that can produce data on actual particle trajectories during such fast processes
455 should also be given a high priority. Also, an interesting issue would be the
456 study of the influence of varying the particle size and density and the particle
457 size distributions on the dust lifting process.

Acknowledgment

The authors thank the Norwegian Research Council (NFR) for funding this research.

References

- Boivin, M., Simonin, O., Squires, D., 2000. On the prediction of gas-solid flows with two-way coupling using large eddy simulations. *Physics of Fluids* 12, 2080-2090.
- Boris, J., Landsberg, A., Oran, E., Gardner, J., 1993. LCPFCT - Flux-

- Corrected Transport algorithm for solving generalized continuity equations.
U.S. Naval Research Laboratory.
- Borisov, A., Sumskoï, S., Komissarov, P., 1999. Experimental and numerical modelling of shock wave interaction with a dust layer. Proceedings of the 17th International Colloquium on the Dynamics of Explosions and Reactive Systems, Heidelberg, Germany.
- Chang, E., Kailasanath, K., 2003. Shock wave interactions with particles and liquid fuel droplets. *Shock Waves* 12, 333-341.
- Clift, R., Gauvin, W., 1970. The motion of particles in turbulent gas streams. *Proceedings Chemeca '70* 1, 14.
- Crowe, C., Sommerfeld, M., Tsuji, Y., 1998. *Multiphase flows with droplets and particles*. CRC Press LLC.
- Fedorov, A.V., Fedorchenko, I.A., 2005. Computation of dust lifting behind a shock wave sliding along the layer. Verification of the model. *Combustion, Explosion, and Shock Waves* 41, 336–345.
- Fedorov, A.V., Gosteev, Y., 2002. Quantitative description of lifting and ignition of organic fuel dusts in shock waves. *Journal of Physics IV* 12, 89–95.
- Fletcher, B., 1976. The interaction of a shock with a dust deposit. *Journal of Physics D—Applied Physics* 9, 197–202.
- Gidaspow, D., 1994. *Multiphase flow and fluidization*. Academic Press.
- Goldschmidt, M., Kuipers, J., van Swaaij, W., 2001. Hydrodynamic modelling of dense gas-fluidised beds using the kinetic theory of granular flow: Effect of coefficient of restitution on bed dynamics. *Chemical Engineering Science* 56, 571-578.
- Henderson, C.B., 1976. Drag coefficients of spheres in continuum and rarefied flows. *AIAA Journal* 14, 707–708.
- Huber, N., Sommerfeld, M., 1998. Modelling and numerical calculation of

- dilute-phase pneumatic conveying in pipe systems. *Powder Technology* 99, 90–101.
- Kauffman, C., Sichel, M., Wolanski, P., 1992. Research on dust explosions at the University of Michigan. *Powder Technology* 71, 119-134.
- Klemens, R., Kosinski, P., Wolanski, P., Korobeinikov, V., Markov, V., Mentshov, I., Semenov, I., 2001. Numerical modelling of coal mine explosion. *Archivum Combustionis* 21.
- Klemens, R., Zydak, P., Kaluzny, M., Litwin, D., Wolanski, P., 2006. Dynamics of dust dispersion from the layer behind the propagating shock wave. *Journal of Loss Prevention in the Process Industries* 19, 200-209.
- Kosinski, P., Hoffmann, A.C., 2005. Modelling of dust lifting using the Lagrangian approach. *International Journal of Multiphase Flow* 31, 1097-1115.
- Kosinski, P., Hoffmann, A.C., Klemens, R., 2005. Dust lifting behind shock waves: Comparison of two modelling techniques. *Chemical Engineering Science* 60, 5219–5230.
- Lebecki, K., Cybulski, K., Sliz, J., Dyduch, Z., Wolanski, P., 1995. Large scale grain dust explosions-research in Poland. *Shock Waves* 5, 109-114.
- Lu, H., Wang, S., Zhao, Y., Yang, L., Gidaspow, D., Ding, J., 2005. Prediction of particle motion in a two-dimensional bubbling fluidized bed using discrete hard-sphere model. *Chemical Engineering Science* 60, 3217–3231.
- Pascal, P., Oesterle, B., 2000. On the dispersion of discrete particles moving in a turbulent shear flow. *International Journal of Multiphase Flows* 26, 293–325.
- Press, W., Teukolsky, S., Vetterling, W., Flannery, B., 1992. *Numerical recipes in FORTRAN 77: The art of scientific computing*. Second edition. Cambridge University Press.
- Saito, T., Marumoto, M., Takayama, K., 2003. Numerical investigations of

- shock waves in gas-particle mixtures. Evaluation of numerical methods for dusty-gas shock wave phenomena. *Shock Waves* 13, 299–322.
- Samuelsberg, A., Hjertager, B., 1996. An experimental and numerical study of flow patterns in a circulating fluidized bed reactor. *International Journal of Multiphase Flow* 22, 575-591.
- Sommerfeld, M., 1992. Modelling of particle-wall collisions in confined gas-particle flows. *International Journal of Multiphase Flow* 18, 905–926.
- Sundaram, S., Collins, L., 1995. Numerical considerations in simulating a turbulent suspension of finite-volume particles. *Journal of Computational Physics* 124, 337–350.
- Suzuki, T., Sakamura, Y., Adachi, T., Kobayashi, S., 1997. Interaction of shock wave with dust layers. *Proceedings of the 21st International Symposium on Shock Waves*, Great Keppel Island, Australia.
- Taniere, A., Khalij, M., Oesterle, B., 2004. Focus on the dispersed phase boundary conditions at the wall for irregular particle bouncing. *International Journal of Multiphase Flow* 30, 327-345.
- Thevand, N., Daniel, E., 2002. Numerical study of the lift force influence on two-phase shock tube boundary layer characteristics. *Shock Waves* 11, 279-288.